Journal of the Optical Society of Korea, Vol. 3, No. 2, September 1999, pp. 55-63

Long-Period Fiber Grating Analysis Using Generalized N×N Coupled-Mode Theory by Section-Wise Discretization

Yoonchan Jeong and Byoungho Lee

School of Electrical Engineering, Seoul National University, Seoul 151-742, KOREA
E-mail: byoungho@snu.ac.kr

(Received May 6, 1999)

For the precise analysis and design of LPFG's, a new method of generalized N×N coupled-mode theory by section-wise discretization was proposed. This is applicable to the analysis for arbitrary grating structures, which can readily take grating nonuniformities and multimode couplings into account. Utilizing the method, several analyses of LPFG's were presented, and relationships between the grating structures and their spectral responses were discussed.

I. INTRODUCTION

Fiber gratings have numerous and important applications in optical fiber sensors and communication systems and have received considerable attention in recent years. Fiber Bragg gratings (FBG's, short-period fiber gratings) currently play important roles in optical fiber systems. As a new feature of fiber grating, a long-period fiber grating (LPFG) was introduced as a band-rejection filter [1], which is also applicable to a fiber sensor [2,3] and an amplified spontaneous emission (ASE) filter or a gain-flattening filter for erbium doped fiber amplifiers (EDFA's) [1,4].

Comparing with FBG's, LPFG's have different properties. As for fabrication [1,5], LPFG's are fabricated, as is depicted in Fig. 1, by ultra-violet (UV) radiation through an amplitude mask, while FBG's are fabricated through a phase mask. As for mode coupling [1,6,7], a propagating core mode is coupled to leaky cladding modes in LPFG's, while to a backward-propagating core mode in FBG's (even though the coupling to cladding modes is possible, the coupling to a backward core mode is dominant unless the grating is tilted). LPFG's are more sensitive to fiber and grating structure than FBG's, because cladding modes, which are expected to be coupled with a fundamental core mode, are more dependent on fiber and grating structure, and more sensitive to external perturbations than the core mode.

The propagation constant differences are shown in Fig. 2 for the core and cladding modes in the unit of length, which is helpful in determining the grating period which is required for resonant coupling. An

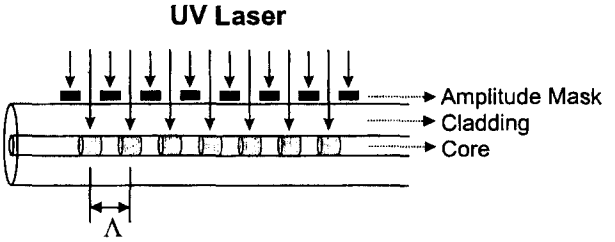

FIG. 1. An LPFG fabrication by UV radiation through an amplitude mask.

LPFG with a grating period Λ is taken as an example, which is indicated by an arrowhead line in Fig. 2. For the LPFG, although the exactly phase-matched wavelength, at which a fundamental core mode can resonantly be coupled to a cladding mode is at λ as shown in Fig. 2(a), the neighboring region, which is denoted by dashed-line ellipses, can be involved in the coupling process due to small phase mismatches. Thus, several-mode couplings can exist due to the narrow mode spacing. That is, the neighborhoods of a resonant mode can be assistants or disturbers for the coupling process. In Fig. 2(a), the vertical dashed-line ellipse denotes the possibility of multimode coupling for a given wavelength, and the horizontal dashed line ellipse denotes the spectral rejection band of the LPFG. As the tangent of the mode-difference line grows, the spectral rejection band becomes narrow in a given length of the LPFG. If mode spacing is sufficiently narrow or the tangent of mode-difference line is sufficiently large at the region of interests, a multiple resonant coupling occurs as depicted with small circles in Fig. 2(b). This

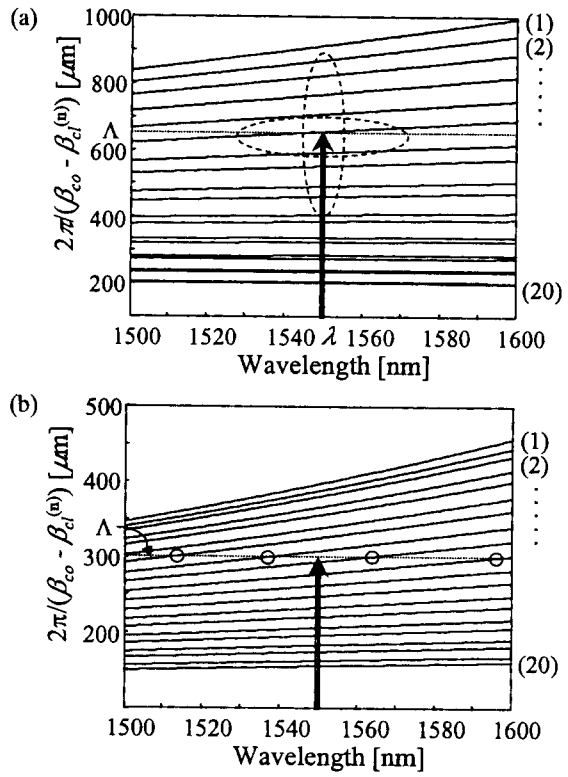

FIG. 2. Propagation-constant differences. (a) For a single-mode fiber (SMF) with core refractive index n_{co} = 1.4514, cladding refractive index n_{cl} = 1.4469, core radius r_{co} = 4 μm, and cladding radius r_{cl} = 62.5 μm (SMF 1). (b) For a SMF with n_{co} = 1.460, n_{cl} = 1.437, r_{co} = 1.3 μm, r_{cl} = 62.5 μm (SMF 2). β_{co} and $\beta_{cl}^{(n)}$ denote the propagation constants of the core mode and the nth cladding mode, respectively. The numbers in the parentheses denote the cladding mode designation number. Λ denotes the LPFG period.

might be desirable or to be avoided according to purposes of applications. In addition, the grating index pattern is not exactly sinusoidal shape due to the fact that LPFG's are fabricated by means of openings of an amplitude mask, as mentioned previously. That is, the wide opening, say hundreds of micrometers, permits the grating structure to have a saturation region of index modulation [7]. Hence, the higher-order terms of Fourier components for the index modulation can nontrivially be involved in mode coupling, since many cladding modes exist readily for them. Therefore, a single-harmonic representation for an LPFG in the coupled-mode equation might not be sufficient for all cases. Furthermore, highly complicated structures of gratings including, for example, phase-shifted, chirped, and superimposed gratings, are required for desirable filter properties. Therefore, the precise analysis of LPFG is truly required so that the multimode couplings can be analyzed in arbitrary grating structures.

Here a new analysis method of generalized N×N coupled-mode theory by section-wise discretization is proposed, which can resolve precise grating structure with a high accuracy and readily consider multimode couplings [8].

II. GENERALIZED N × N COUPLED-MODE THEORY BY SECTION-WISE DISCRETIZATION

The coupled-mode equation induced from Lorentz reciprocity [9] is given by (see APPNEDIX A)

$$\nabla \cdot (\mathbf{E}' \times \mathbf{H}_p^* + \mathbf{E}_p^* \times \mathbf{H}') = -i\omega \mathbf{E}_p^* \cdot \Delta\epsilon \mathbf{E}', \; p = 1, 2, ... \tag{1}$$

where the terms subscripted by p denote the pth eigenmode including either core or cladding mode, and the terms superscripted by a prime denote the perturbed mode which is represented by a sum of eigenmodes multiplied by variation constants. $\Delta\epsilon$ and $*$ represent the permittivity perturbation and the complex conjugate, respectively. The permittivity perturbation, i.e., the imposed index modulation can vary both transversely and longitudinally. Relative to the variation of index modulation along the fiber axis (z direction), it can be represented as depicted in Fig. 3(a). When the permittivity perturbation is an arbitrary function of z position, it would be cumbersome to solve the

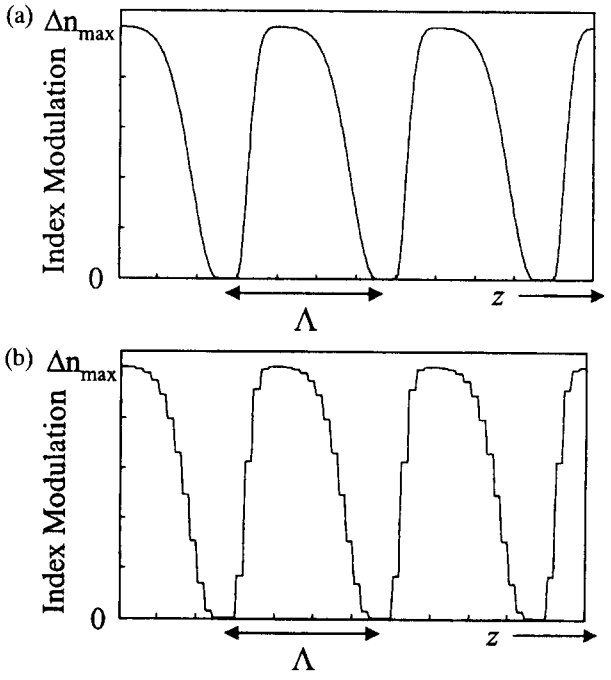

FIG. 3. (a) Index modulation in fiber core and (b) its discretization. Λ denotes the grating period. Note that the asymmetric shape of the index modulation illustrates a possibility for an arbitrary grating shape.

coupled equation analytically. However, if the permittivity perturbation $\Delta\epsilon$ is regarded as constant in each finite section relative to the z direction, as is depicted in Fig. 3(b), the coupled equation is represented by an ordinary linear differential equation within the specified section. This can be solved easily, regardless of mode numbers and complexity of the grating structure. In this respect, we call the discretizing of the permittivity variation and solving (1) with multiple modes as "generalized N×N coupled-mode theory by section-wise discretization". It is noteworthy that the dependence on transverse coordinates in $\Delta\epsilon$ can be estimated to an average value by applying overlap integration in the plane transverse to the z direction. By cascading the solution in each finite section, the entire analysis of fiber gratings can be accomplished with proper relations at section boundaries. If the fiber grating has a uniform periodicity, it is sufficient to calculate just for one period of the refractive index change. In general, even in the grating structure having no periodicity, the method can readily be applied in the analysis. In addition, there is no need for representing the grating structure with a Fourier series or a Fourier integral, since the proposed method represents it realistically by appropriate discretizations of the optical quantities. Hence, the grating representation problem in the case of finite-length gratings is excluded. Proper discretization with a consideration of the degree of index variation can give sufficiently accurate results. The entire calculations are performed by matrix algebra as follows.

Let us suppose that the pth eigenmode, which can be either core or cladding mode, is given by

$$\mathbf{E}_p = \mathbf{e}_p(r,\phi)\exp(-i\beta_p z) \tag{2}$$

where $\mathbf{e}_p(r,\phi)$ is the electric field vector which is normalized to a power flow of 1 W in the z direction, r and ϕ denote the polar coordinates in the plane transverse to the z direction, and β_p denotes the propagation constant in the z direction. The perturbed electric field is supposed to be

$$\mathbf{E}'(m) = \sum_q a_q(z;m)\mathbf{e}_p(r,\phi)\exp(-i\beta_q z) \tag{3}$$

where the argument m denotes the mth discretized section relative to the z direction. Substituting (3) into (1), along with the discretized quantity of $\Delta\epsilon(m)$, the coupled equation of (1) is changed to (see APPENDIX B)

$$\frac{d\mathbf{A}(z;m)}{dz} = -i\left(\mathbf{B}+\frac{\omega}{4}\mathbf{M}(m)\right)\cdot\mathbf{A}(z;m) \equiv \mathbf{D}(m)\cdot\mathbf{A}(z;m), \tag{4}$$

where $\mathbf{A}$ is a column vector whose elements are $A_{(p)}(p=1,2,...)$, and $\mathbf{B}$ and $\mathbf{M}$ are matrices, whose (p,q) elements are $B_{(p,q)}$ and $M_{(p,q)}$, respectively:

$$A_{(p)}(z;m) = a_p(z;m)\exp(-i\beta_p z) \tag{5.a}$$

$$B_{(p,q)} = \begin{cases} \beta_p, & p=q \\ 0, & p\neq q \end{cases} \tag{5.b}$$

$$M_{(p,q)} = \int \mathbf{e}_p^*\cdot\epsilon(m)\mathbf{e}_q dS \tag{5.c}$$

where dS denotes surface integral element in the plane transverse to the z direction.

It is noteworthy that there is no z variation in $\mathbf{D}(m)$, because the permittivity variation along the z direction has readily been discretized with $\Delta\epsilon(m)$ in the mth section. Hence, (4) can be solved to a transfer relation form by means of finding eigenvalues and correspondent eigenvectors of the matrix $\mathbf{D}(m)$ as follows:

$$\mathbf{A}(z_f;m) = \mathbf{V}(m)\cdot\exp[\mathbf{U}(m)\cdot(z_f-z_i)]\cdot\mathbf{V}(m)^{-1}\cdot\mathbf{A}(z_i;m) \equiv \mathbf{T}(m)\cdot\mathbf{A}(z_i;m) \tag{6}$$

where z_i and z_f denote the left-end and the right-end positions of the mth section, respectively, and $\mathbf{U}(m)$ and $\mathbf{V}(m)$ denote the diagonal eigenvalue matrix of $\mathbf{D}(m)$ and the corresponding eigenvector matrix, respectively. Since $\mathbf{A}(z_i;m+1)$ equals to $\mathbf{A}(z_f;m)$ for the given notation, the overall transfer relation through the entire cascading sections can be constructed as follows:

$$\mathbf{A}^{right} = \cdots\mathbf{T}(m+1)\cdot\mathbf{T}(m)\cdot\mathbf{T}(m-1)\cdots\mathbf{T}(1)\cdot\mathbf{A}^{left}. \tag{7}$$

Therefore, the overall spectral response of the fiber grating can be obtained by cascading the transfer relations for discretized sections with initial incident conditions. In other words, this method can be stated as an extended concept of the transfer matrix method [6,10], which has widely been being used in analyzing nonuniform gratings. While the transfer matrix method regards a nonuniform grating as a series of slightly different but uniform gratings, the proposed method represents it realistically by discretizing its precise structure regardless of uniformity. Thus, it can resolve the nonuniformity into an amount less than one grating period. When using this method, it is not required to consider which mode is coupled and to select dominant-coupling constant, and multimode couplings can easily be resolved. That is, the mode selection rule [6,7] is no longer required. Only the proper discretization of optical quantities is required in representing the grating structure.

III. NUMERICAL RESULTS

In the calculations, it is assumed that the fiber is a common single-mode fiber. Thus, the eigenmodes for core and cladding mode are chosen as HE_{11} core mode

and the cladding modes that have the same ϕ variation with that of the core mode, respectively, since the overlap integral matrix **M** has non-zero values for the same ϕ variation unless the gratings are tilted [6] (note that other cladding modes can be included if $\Delta\epsilon(m)$ has ϕ variation, for example, in cases of tilted fiber gratings). The mathematical expressions of fiber modes are represented by the Bessel functions of the first and second kind, and the modified Bessel functions of the second kind according to region [7,11]. The modes are determined by solving characteristic equations from the continuity relations for tangential E- and H-field at the boundaries. The dimensions of the characteristic matrix equations are 4×4 for core mode, and 8×8 for cladding mode, respectively.

Fig. 2, previously shown, represents the eigenmodes determined by the characteristic equations for the given fibers surrounded by air. Fig. 4 shows the several overlap-integral values of E-fields (within core region) between the core and cladding mode (excluding $\Delta\epsilon(m)$ multiplication). It can be seen that the integral values depend on the mode orders, which have the role of coupling efficiency, as well as the index modulation depth does. In order to achieve the efficient coupling, it is desirable to determine the grating period such that the overlap-integral value is sufficiently large on resonant coupling condition. The tangent of the mode-difference line is also required to be precisely considered for the spectral rejection band determination, which is also dependent on wavelength, grating length, and mode effective index [1,6].

When discretizing the optical quantities through the grating, it is assumed that the saturated index region is a half of an amplitude-mask opening, and each falling and rising index region is a quarter of it. The profile of refractive index change is modeled by a six-order super-Gaussian function and discretized with 2^6 discrete sections per period unless stated otherwise.

Fig. 5 shows calculated results using the proposed method with twenty-one modes, i.e., with one core mode and twenty cladding modes (hereafter, the mode set is assumed to be composed of twenty-one eigenmodes). In principle, this is an extensive consideration of multimode couplings. In practice, not necessarily all, but several of cladding modes, which are nearest-neighboring modes along the resonant coupling condition, are required for the appropriate calculation [6]. It can be seen that the rejection band moves to longer wavelengths as the index modulation depth grows [1], which is due to the fact that the mode-difference lines,

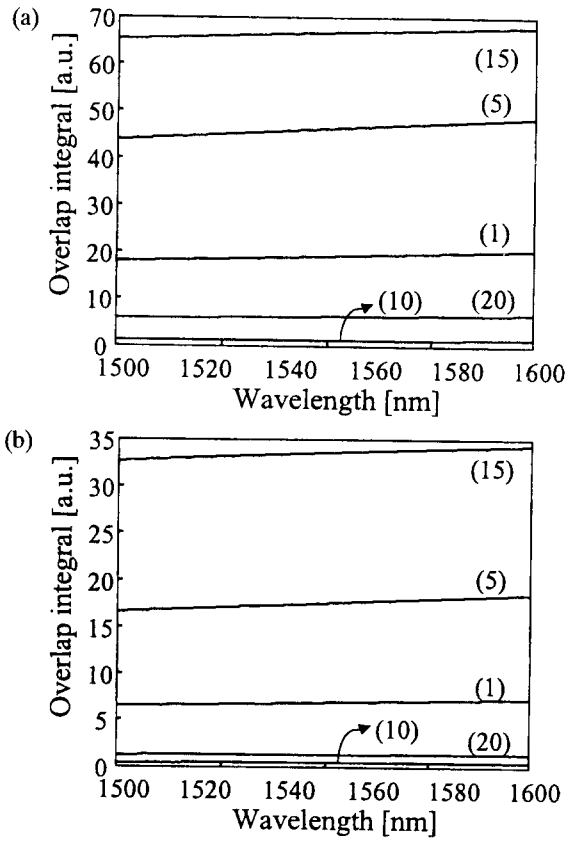

FIG. 4. Overlap integral values of E-fields in the core region between the core and cladding mode for (a) SMF 1, (b) SMF 2. The numbers in the parentheses denote the designation number of cladding mode.

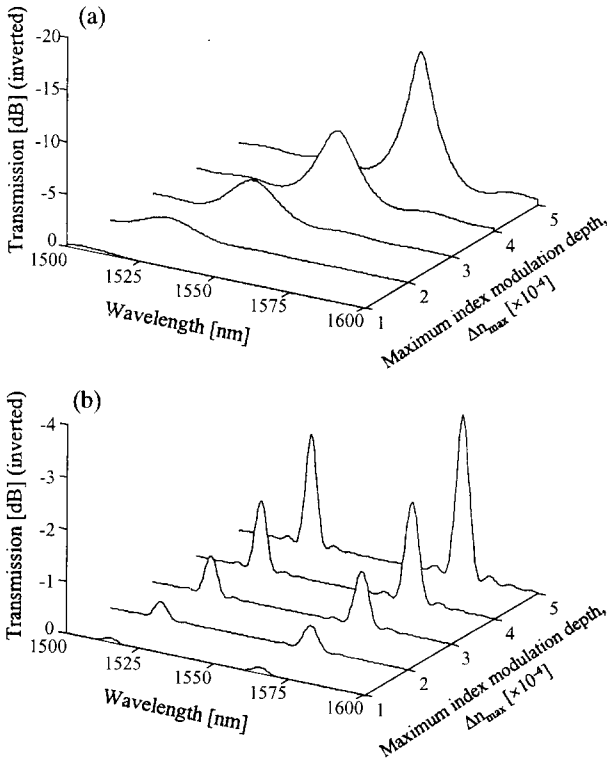

FIG. 5. Spectral responses of transmission through LPFG's for various index modulation depths (a) on SMF 1, $\Lambda = 660$ μm, 1 inch-long, (b) on SMF 2, $\Lambda = 300$ μm, and 1 inch-long. Note that the graphs are inverted for an ease of visualization, i.e., the transmission becomes smaller along the vertical axes of the graphs.

as depicted in Fig. 2, are effectively contracted downward as the index modulation depth increases, i.e., the effective indices increase. Comparing Figs. 5(a) and 5(b), several differences can be seen. In the case of Fig. 5(b), the amount of band rejection is smaller than that of the case of Fig. 5(a). This is due to the difference in the overlap-integral value between the coupling modes. Even though they are dependent on the mode order as mentioned previously, they are also dependent on the core size if other conditions are fixed. That is, as the core size increases, the fraction of interaction region for the core and cladding modes is increased relatively. In the case of Fig. 5(b), the amount of band shift is smaller than that in the case of Fig. 5(a). This is due to the fact that the effective index increment in the case of Fig. 5(b) is smaller than that in the case of Fig. 5(a) with the same index modulation depth increment. Note that the effective index increment is proportional to the product of index modulation and overlap integral value. Thus, contraction of the mode-difference line for the case of Fig. 5(b) is relatively insensitive to the increment of index modulation depth, because the overlap integral values are relatively small comparing with the case of Fig. 5(a). For auto-overlap integral, the value for the case of Fig. 5(b) is smaller than that for the case of Fig. 5(a), because of smaller V-parameter value [11]. When the V-parameter value is relatively large, the core mode is well confined in the core region, hence permitting large auto- and cross-overlap integrals, which are relative to the amounts of rejection-band shift and depth, respectively. In addition, it can be seen in Fig. 5(b) that there exist two rejection bands in the given spectral region. In Fig. 2(b), it can be seen that there are multiple resonant coupling points. However, only two resonant couplings are dominant, since others have relatively smaller overlap integral values, which, in fact, are EH-like modes.

Fig. 6 shows the band-rejection properties for various duty ratios (high-index region versus low-index region) of the opening and the closing in an amplitude mask with a fixed period. It can be seen that the rejection band moves to longer wavelengths as the duty ratio increases. This is due to the fact that the effective indices are increased as the duty ratio increases, which is similar to the case of index modulation increment, as in Fig. 5. However, the shape of the rejection band becomes distorted as the duty ratio deviates from the ratio (5 : 5). As the duty ratio deviates from the symmetry, higher-order components of spatial Fourier harmonics becomes nontrivial, thereby permitting their contribution to the spectral response.

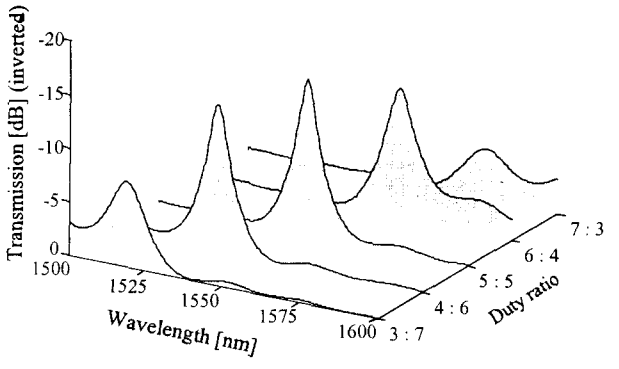

FIG. 6. Spectral responses of transmission through LPFG's on SMF 1 for various duty ratios of the opening and the closing in an amplitude mask: $\Delta n_{max} = 5 \times 10^{-4}$, $\Lambda = 660\mu$m, and 1 inch-long.

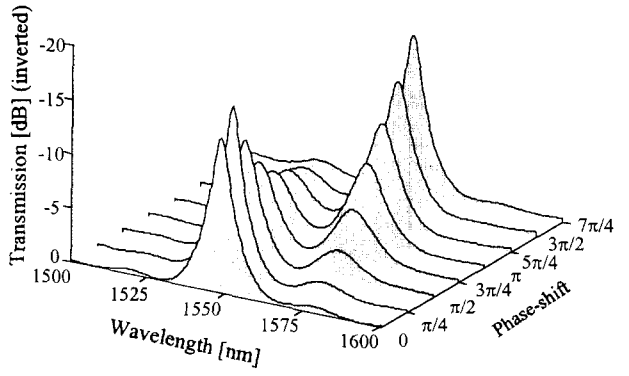

FIG. 7. Spectral responses of transmission through LPFG's on SMF 1 for various phase shifts at the center position of each LPFG: $\Delta n_{max} = 5 \times 10^{-4}$, $\Lambda = 660\ \mu$m, and 1 inch-long.

Fig. 7 shows the band-rejection properties according to the grating phase shift at the center position of a uniform LPFG. As the phase shift increases, the rejection-band lobe in the longer wavelength region becomes large, and the overall band moves simultaneously to shorter wavelengths. At phase shift of π, the rejection band becomes split to the center of the non-phase-shifted one, which is like a band-pass filter [12].

This phenomenon can be interpreted as follows. Since the phase shift is placed at the center position of the LPFG, the LPFG can be regarded as a composition of three parts; two identical uniform periodic gratings in both sides and a small one, which gives the phase shift, at center (see Fig. 8). Thus, the phase-shift part at center can be regarded as a perturbation in a uniform LPFG, since the uniform ones in both sides are identical. If the phase-shift position is not at center, the length ratio of uniform gratings in both sides must be considered as a perturbation factor. Mathematically, this is due to the multiplication order of transfer matrices. That is, the transfer matrix for the phase-shift part (see (7)) does not commute with that of the uniform grating; thus, the imbedding position can also be a primary factor. Hereafter, let us primarily discuss the case that the phase-shift part is located at center. The grating length of the phase-shift part, which is a perturbation to the uniform grating with

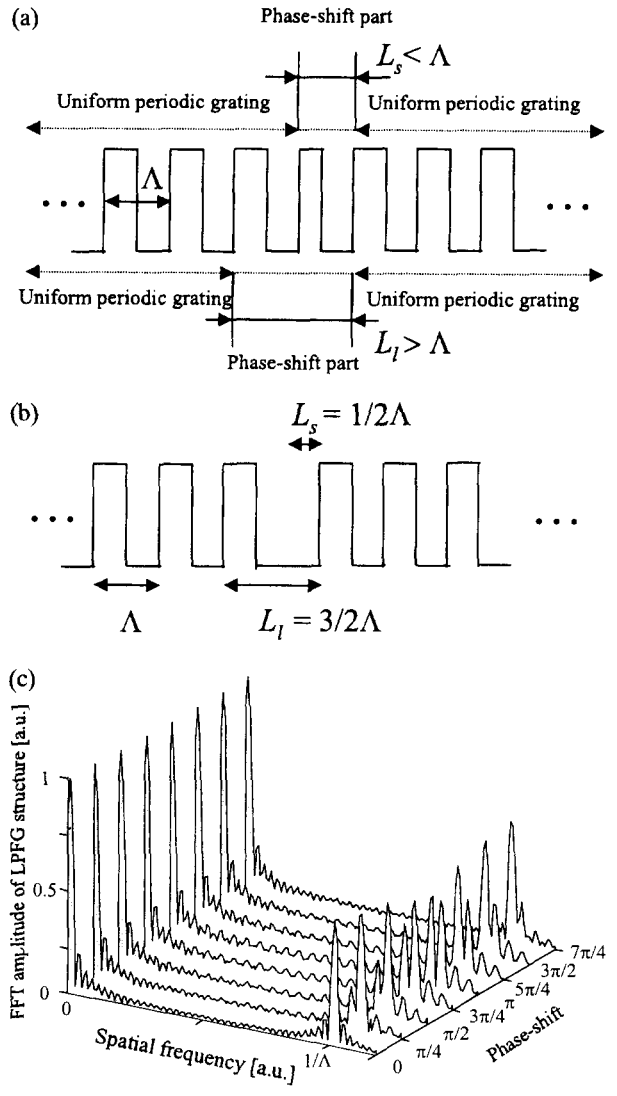

FIG. 8. Interpretation of phase-shift part and Fourier transform of the overall index profile (a) for the phase shift less than π and (b) for the phase shift π. L_s and L_l denote the lengths of the phase-shift grating when it is regarded as a shorter grating and as a longer one, respectively. (c) Fourier transform of the overall index profile in phase-shifted LPFG by means of FFT.

violation of the grating sequence, can be treated as in two ways; a shorter or a longer grating, as shown in Fig. 8. Therefore, the overall effective (averaged) period of gratings can be interpreted as reduced or enlarged, respectively. Up to phase shift π, its playing as a shorter one is dominant rather than as a longer one, since the phase-mismatch amount of the former case is smaller than that of the latter case. However, its playing as a longer one becomes larger as the phase shift increases, which results in the increment of the rejection-band lobe in the longer wavelength region. By the way, both the shorter and the longer one lose their lengths as phase shift increases, and, hence, each rejection band moves to shorter wavelengths. If the phase shift becomes π, the phase-shift part in the absence of a half period can be interpreted as either a half-period or a one-and-half-period grating, since it is attached to the former grating sequence enlarging the tail, as depicted in Fig. 8(b). Then, the alternative effects are balanced; thus, the rejection band becomes split symmetrically to the center of a rejection band in the case of a non-phase-shifted grating, except the precise rejection amount that is dependent on the overlap integral value according to wavelengths. After phase shift π, the effect of a longer one exceeds that of a shorter one; thus, the rejection-band lobe in the longer wavelength region increases furthermore and moves simultaneously to shorter wavelengths, and finally, it returns back to the non-phase-shifted case at phase shift 2π.

Alternatively, this concept can be verified by Fourier-transform analysis. Fig. 8(c) shows the Fourier transform of the overall phase-shifted grating, which has been calculated by the fast Fourier transform method (FFT) with the discretized profile of the index modulation. In Fig. 8(c), peaks at spatial frequencies zero and $1/\Lambda$ denote dc and first-order components of the FFT result, respectively. The first-order peak at $1/\Lambda$ represents the effective period. Second-, third-, and higher-order peaks follow after; however, they are omitted for ease of visualization. It can be seen that the peak at $1/\Lambda$ becomes split into two competing parts as the phase shift increases. That is, the effective grating period becomes shorter or longer, as has been mentioned. Each peak produces a rejection-band lobe according to its amplitude. In addition, it can be seen that the peak becomes split symmetrically at phase shift π. The envelopes follow the trend as was discussed previously.

The realization of EDFA gain-flattening filter with LPFG requires a precise design technique. The fil-

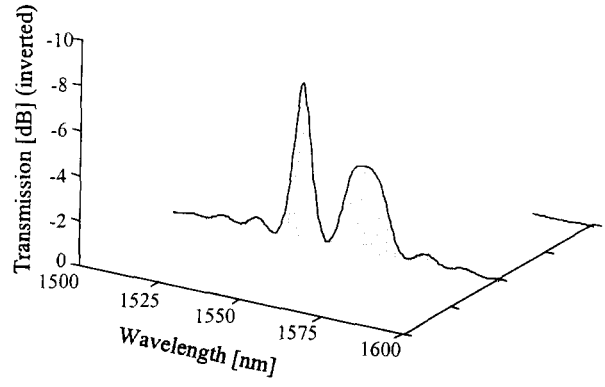

FIG. 9. Spectral responses of transmission through a superimposed LPFG with $\Delta n_{max} = 5 \times 10^{-4}$. The superimposed grating periods are 645 μm, 655 μm, and 660 μm, corresponding ratio of index modulation depths is (5.0 : 3.5 : 4.5), and the grating is 2-inch long.

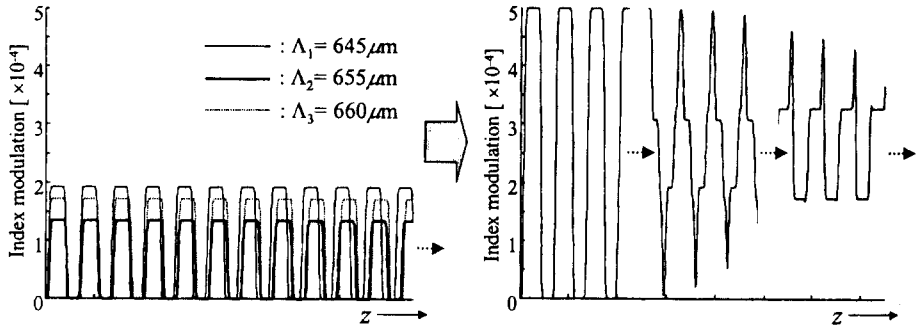

FIG. 10. Index modulation profile of the superimposed LPFG. Superposition of each index modulation in left graph results in a complex index profile in right one.

ter can be implemented with nonuniform gratings such as chirped, phase-shifted, superimposed, and cascade types, according to specific filtering properties. For example, the spectral response of a superimposed grating has been analyzed in Fig. 9(a) using the proposed method with a resolution of 1-mm-long discrete section. This can be realized by multiple exposure of UV radiation with several different-period masks or by a single integrated mask. It is assumed that the grating is superimposed by three different period gratings, the index modulation of which are depicted in Fig. 9(b). It can be seen that the superposition of three gratings, whose grating periods are 645 μm, 655 μm, and 660 μm, respectively, produces a wide rejection band around wavelength 1560 nm on the right side of the normal rejection band at wavelength 1535 nm.

The analysis of nonuniform gratings like this example can be complicated by conventional coupled-mode theory. The proposed method can resolve them by means of section-wise discretization of the complex optical quantities, regardless of their complexities. Therefore, the proposed method can be useful as an analysis method for the precise LPFG design in the cases of nonuniform gratings and multimode-coupling regimes. In contrast to the easy treatment of highly nonuniform gratings, the calculation time, however, becomes slower when the length of a discretization section is shortened, and the number of modes which are involved in the calculation increases.

IV. CONCLUSION

For precise analysis of LPFG's, the generalized N × N coupled-mode theory by section-wise discretization has been proposed. The validity and versatility of this method have been verified by several numerical examples. It can be seen that the spectral response of an LPFG is more dependent on fiber and grating parameters than for an FBG. Understanding the nature of LPFG's with the proposed method can be a guide to an LPFG design. In addition, the proposed method is applicable to the analysis of FBG's, distributed Bragg reflector (DBR) lasers, distributed feed back (DFB) lasers, and other grating devices, as well as to that of LPFG's.

ACKNOWLEDGMENTS

The authors acknowledge the support of the Ministry of Science and Technology of Korea through Korea Telecom and KAIST.

REFERENCES

[1] A. M. Vengsarkar, P. J. Lemaire, J. B. Judkins, V. Bhatia, T. Erdogan, and J. E. Sipe, J. Lightwave Technol. **14**, 58 (1996).
[2] V. Bhatia and A. M. Vengsarkar, Opt. Lett. **21**, 692 (1996).
[3] H. J. Patrick, G. M. Williams, A. D. Kersey, J. R. Pedrazzani, and A. M. Vengsarkar, IEEE Photon. Technol. Lett. **8**, 1223 (1996).
[4] P. F. Wysocki, J. Judkins, R. Espindola, M. Andrejco, A. Vengsarkar, and K. Walker, in Optic. Fiber Commun.Conf., (Dallas, TX, Feb. 16-21, 1997), paper PD2.
[5] K. O. Hill, B. Malo, F. Bilodeau, D. C. Johnson, and J. Albert, Appl. Phys. Lett. **62**, 1035 (1993).
[6] T. Erdogan, J. Lightwave Technol. **15**, 1277 (1997).
[7] Y. Zhao and J. C. Palais, J. Lightwave Technol. **15**, 154 (1997).
[8] Y. Jeong and B. Lee, in Proc. Conf. Lasers and Electro-Opt. Europe, (Glasgow, Scotland, U.K., Sept. 14-18, 1998), paper CWF62.
[9] A. Yariv and P. Yeh, *Optical Waves in Crystals. New York* (Wiley, 1984).
[10] M. Yamada and K. Sakuda, Appl. Opt. **26** 3474 (1987).
[11] A. Yariv, *Optical Electronics* (Saunders College Publishing, New York, 1991) 3rd ed.
[12] F. Bakhti and P. Sansonetti, in Optic. Fiber Commun.Conf., (Dallas, TX, Feb. 16-21, 1997) paper FB4.

APPENDIX A

For complex-valued amplitudes, Lorentz reciprocity theorem is represented by [9]

$$\nabla \cdot (\mathbf{E}_q \times \mathbf{H}_p^* + \mathbf{E}_p{}^* \times \mathbf{H}_q) = 0,\ p,q = 1,2,... \tag{A1}$$

where p and q denote the eigenmode designation numbers. The eigenmode denotes the orthogonal mode which can exist in a lossless medium represented by permittivity ϵ and permeability μ. Let us suppose that a certain perturbation exists in the permittivity ϵ; thus, the permittivity is changed to ϵ' , which can be represented by the sum of an unperturbed term ϵ and a perturbed term $\Delta\epsilon$, i.e., $\epsilon' = \epsilon + \Delta\epsilon$ (assuming no change in permeability μ). Then, let us assume that the perturbed fields in the medium of ϵ' are represented by $\mathbf{E}'$ and $\mathbf{H}'$. Substituting $\mathbf{E}_q$ and $\mathbf{H}_q$ with $\mathbf{E}'$ and $\mathbf{H}'$ in the left-hand side (*LHS*) of (A1) leads to

$$LHS = \nabla \cdot (\mathbf{E}' \times \mathbf{H}_p^* + \mathbf{E}_p^* \times \mathbf{H}'). \tag{A2}$$

After manipulating (A2), it follows that

$$LHS = -i\omega(\mathbf{E}_p^* \cdot \mathbf{D}' - \mathbf{E}' \cdot \mathbf{D}_p^* + \mathbf{H}_p^* \cdot \mathbf{B}' - \mathbf{H}' \cdot \mathbf{B}_p^*) \tag{A3}$$

where $\exp(i\omega t)$ excitation is assumed, and $\mathbf{D}$ and $\mathbf{B}$ denote the corresponding displacement vector and magnetic flux density, respectively. Applying the constitutive relations, i.e., $\mathbf{D}_p = \epsilon\mathbf{E}_p$, $\mathbf{D}' = \epsilon'\mathbf{E}' = (\epsilon + \Delta\epsilon)\mathbf{E}'$, $\mathbf{B}_p = \mu\mathbf{H}_p$, and $\mathbf{B}' = \mu\mathbf{H}'$, to (A3), it follows that

$$\nabla \cdot (\mathbf{E}' \times \mathbf{H}_p^* + \mathbf{E}_p^* \times \mathbf{H}') = -i\omega\mathbf{E}_p^* \cdot \Delta\epsilon\mathbf{E}'. \tag{A4}$$

If $\Delta\epsilon$ is zero, $\mathbf{E}'$ and $\mathbf{H}'$ become the eigenmode fields for the unperturbed medium ϵ , and, hence, the right-hand side of (A4) becomes zero. As expected, (A4) becomes (A1) if $\Delta\epsilon = 0$. Therefore, the derivation of coupled-mode equation is completed.

APPENDIX B

Assuming slowly varying amplitudes with the variation constant method [9], the perturbed fields $\mathbf{E}'$ and $\mathbf{H}'$ can be represented, without losing generality, as follows:

$$\begin{pmatrix} \mathbf{E}'(m) \\ \mathbf{H}'(m) \end{pmatrix} = \sum_q a_q(z;m) \begin{pmatrix} \mathbf{E}_q(m) \\ \mathbf{H}_q(m) \end{pmatrix} = \sum_q a_q(z;m) \begin{pmatrix} \mathbf{e}_p(r,\phi)\exp(-i\beta_q z) \\ \mathbf{h}_p(r,\phi)\exp(-i\beta_q z) \end{pmatrix} \tag{B1}$$

where $\mathbf{E}_q$ and $\mathbf{H}_q$ denote the fields for the qth eigenmode, whose electric field vector $\mathbf{e}_q(r,\phi)$ and magnetic field vector $\mathbf{h}_q(r,\phi)$ are normalized to a power flow of 1 W in the z direction, and m denotes the mth discretized section. Substituting (B1) into (1) with the discretized permittivity perturbation $\Delta\epsilon(m)$ yields

$$\sum_q a_q(z;m)\nabla \cdot (\mathbf{E}_q \times \mathbf{H}_p^* + \mathbf{E}_p{}^* \times \mathbf{H}_q) + \sum_q \frac{da_q(z;m)}{dz}(\mathbf{E}_q \times \mathbf{H}_p^* + \mathbf{E}_p{}^* \times \mathbf{H}_q) \cdot \hat{z} \tag{B2}$$
$$= -i\omega \sum_q a_q(z;m)\mathbf{E}_p^* \cdot \Delta\epsilon(m)\mathbf{E}_q,\ p = 1,2,...$$

where $\hat{z}$ denotes a unit vector along the z direction. It can be seen that the first summation in the left-hand side of (B2) vanishes by means of Lorentz reciprocity theorem of (A1). Applying surface integration on both sides of (B2) in the plane transverse to the z direction, it follows that

$$\frac{da_q(z;m)}{dz}\exp(-i\beta_p z) = -i\frac{\omega}{4}\sum_q a_q(z;m)\exp(-i\beta_q z)\int \mathbf{e}_p^* \cdot \Delta\epsilon(m)\mathbf{e}_q dS,\ p = 1,2,... \tag{B3}$$

where dS denotes the surface integral element in the plane transverse to the z direction, and the power normalization [1], i.e.,

$$\frac{1}{4}\int(\mathbf{E}_q \times \mathbf{H}_p^* + \mathbf{E}_p^* \times \mathbf{H}_q)\cdot \hat{z}dS = \begin{cases} 1, & p = q \\ 0, & p \neq q \end{cases} \tag{B4}$$

has readily been utilized. Therefore, (B3), along with (5), leads to

$$\frac{d\mathbf{A}(z;m)}{dz} = -i\left(\mathbf{B} + \frac{\omega}{4}\mathbf{M}(m)\right)\cdot \mathbf{A}(z;m) \equiv \mathbf{D}(m)\cdot \mathbf{A}(z;m). \tag{B5}$$